

Image Restoration by Iterative Denoising and Backward Projections

Tom Tirer, and Raja Giryes

Abstract

Inverse problems appear in many applications such as image deblurring and inpainting. The common approach to address them is to design a specific algorithm for each problem. The Plug-and-Play (P&P) framework, which has been recently introduced, allows solving general inverse problems by leveraging the impressive capabilities of existing denoising algorithms. While this fresh strategy has found many applications, a burdensome parameter tuning is often required in order to obtain high-quality results. In this work, we propose an alternative method for solving inverse problems using denoising algorithms, that requires less parameter tuning. We provide theoretical analysis of the method, and empirically demonstrate that it is competitive with task-specific techniques and the P&P approach for image inpainting and deblurring.

Index Terms

Plug-and-Play, inverse problems, image restoration, image denoising

I. INTRODUCTION

We consider the reconstruction of an image from its degraded version, which may be noisy, blurred, downsampled, or all together. This general problem has many important applications, such as medical imaging, surveillance, entertainment, and more. Traditionally, the design of task-specific algorithms has been the ruling approach. Many works specifically considered the denoising problem [1]–[3], the deblurring problem [4]–[6], the inpainting problem [7], [8], etc.

Recently, a new approach attracts much interest. This approach suggests leveraging the impressive capabilities of existing denoising algorithms for solving other tasks that can be formulated as an inverse problem. The pioneering algorithm that introduced this concept is the Plug-and-Play (P&P) method [9], which presents an elegant way to decouple the measurement model and the image prior, such that the latter is handled solely by a denoising operation. Thus, it is not required to explicitly specify the prior, since it is implicitly defined through the choice of the denoiser.

The authors are with the School of Electrical Engineering, Tel Aviv University, Tel Aviv 69978, Israel. (email: tirer.tom@gmail.com, raja@tauex.tau.ac.il)

The P&P method has already found many applications, e.g. bright field electron tomography [10], Poisson denoising [11], and postprocessing of compressed images [12]. It also inspired new related techniques [13]–[15]. However, it has been noticed that the P&P often requires a burdensome parameter tuning in order to obtain high quality results [14], [16]. Moreover, since it is an iterative method, sometimes a large number of iterations is required.

In this work, we propose a simple iterative method for solving linear inverse problems using denoising algorithms, which provides an alternative to P&P. Our strategy has less parameters that require tuning (e.g. no tuning is required for the noisy inpainting problem), often requires less iterations, and its recovery performance is competitive with task-specific algorithms and with the P&P approach. We demonstrate the advantages of the new technique on inpainting and deblurring problems.

The paper is organized as follows. In Section II we present the problem formulation and the P&P approach. The proposed algorithm is presented in Section III. Section IV includes mathematical analysis of the algorithm and provides a practical way to tune its parameter. In Section V the usage of the method is demonstrated and examined for inpainting and deblurring problems. Section VI concludes the paper.

II. BACKGROUND

A. Problem formulation

The problem of image restoration can be generally formulated by

$$\mathbf{y} = \mathbf{H}\mathbf{x} + \mathbf{e}, \quad (1)$$

where $\mathbf{x} \in \mathbb{R}^n$ represents the unknown original image, $\mathbf{y} \in \mathbb{R}^m$ represents the observations, \mathbf{H} is an $m \times n$ degradation matrix and $\mathbf{e} \in \mathbb{R}^m$ is a vector of independent and identically distributed Gaussian random variables with zero mean and standard deviation of σ_n . The model in (1) can represent different image restoration problems; for example: image denoising when \mathbf{H} is the $n \times n$ identity matrix \mathbf{I}_n , image inpainting when \mathbf{H} is a selection of m rows of \mathbf{I}_n , and image deblurring when \mathbf{H} is a blurring operator.

In all of these cases, a prior image model $s(\mathbf{x})$ is required in order to successfully estimate \mathbf{x} from the observations \mathbf{y} . Specifically, note that \mathbf{H} is ill-conditioned in the case of image deblurring, thus, in practice it can be approximated by a rank-deficient matrix, or alternatively by a full rank $m \times n$ matrix ($m < n$). Therefore, for a unified formulation of inpainting and deblurring problems, which are the test cases of this paper, we assume $m < n$.

Almost any approach for recovering \mathbf{x} involves formulating a cost function, composed of fidelity and penalty terms, which is minimized by the desired solution. The fidelity term ensures that the solution agrees with the measurements, and is often derived from the negative log-likelihood function. The penalty term regularizes the optimization problem through the prior image model $s(\mathbf{x})$. Hence, the typical cost function is

$$f(\tilde{\mathbf{x}}) = \frac{1}{2\sigma_n^2} \|\mathbf{y} - \mathbf{H}\tilde{\mathbf{x}}\|_2^2 + s(\tilde{\mathbf{x}}), \quad (2)$$

where $\|\cdot\|_2$ stands for the Euclidean norm.

B. Plug and Play approach

Instead of devising a separate algorithm to solve $\min_{\tilde{\mathbf{x}}} f(\tilde{\mathbf{x}})$ for each type of matrix \mathbf{H} , a general recovery strategy has been proposed in [9], denoted as the Plug-and-Play (P&P). For completeness, we briefly describe this technique.

Using variable splitting, the P&P method restates the minimization problem as

$$\min_{\tilde{\mathbf{x}}, \tilde{\mathbf{v}}} \ell(\tilde{\mathbf{x}}) + \beta s(\tilde{\mathbf{v}}) \quad \text{s.t.} \quad \tilde{\mathbf{x}} = \tilde{\mathbf{v}}, \quad (3)$$

where $\ell(\tilde{\mathbf{x}}) \triangleq \frac{1}{2\sigma_n^2} \|\mathbf{y} - \mathbf{H}\tilde{\mathbf{x}}\|_2^2$ is the fidelity term in (2), and β is a positive parameter that adds flexibility to the cost function. This problem can be solved using ADMM [17] by constructing an augmented Lagrangian, which is given by

$$\begin{aligned} L_\lambda &= \ell(\tilde{\mathbf{x}}) + \beta s(\tilde{\mathbf{v}}) + \mathbf{u}^T(\tilde{\mathbf{x}} - \tilde{\mathbf{v}}) + \frac{\lambda}{2} \|\tilde{\mathbf{x}} - \tilde{\mathbf{v}}\|_2^2 \\ &= \ell(\tilde{\mathbf{x}}) + \beta s(\tilde{\mathbf{v}}) + \frac{\lambda}{2} \|\tilde{\mathbf{x}} - \tilde{\mathbf{v}} + \tilde{\mathbf{u}}\|_2^2 + \frac{\lambda}{2} \|\tilde{\mathbf{u}}\|_2^2, \end{aligned} \quad (4)$$

where \mathbf{u} is the dual variable, $\tilde{\mathbf{u}} \triangleq \frac{1}{\lambda} \mathbf{u}$ is the scaled dual variable, and λ is the ADMM penalty parameter. The ADMM algorithm consists of iterating until convergence over the following three steps

$$\begin{aligned} \tilde{\mathbf{x}}_k &= \underset{\tilde{\mathbf{x}}}{\operatorname{argmin}} L_\lambda(\tilde{\mathbf{x}}, \tilde{\mathbf{v}}_{k-1}, \tilde{\mathbf{u}}_{k-1}), \\ \tilde{\mathbf{v}}_k &= \underset{\tilde{\mathbf{v}}}{\operatorname{argmin}} L_\lambda(\tilde{\mathbf{x}}_k, \tilde{\mathbf{v}}, \tilde{\mathbf{u}}_{k-1}), \\ \tilde{\mathbf{u}}_k &= \tilde{\mathbf{u}}_{k-1} + (\tilde{\mathbf{x}}_k - \tilde{\mathbf{v}}_k). \end{aligned} \quad (5)$$

By plugging (4) in (5) we have

$$\begin{aligned} \tilde{\mathbf{x}}_k &= \underset{\tilde{\mathbf{x}}}{\operatorname{argmin}} \ell(\tilde{\mathbf{x}}) + \frac{\lambda}{2} \|\tilde{\mathbf{x}} - (\tilde{\mathbf{v}}_{k-1} - \tilde{\mathbf{u}}_{k-1})\|_2^2, \\ \tilde{\mathbf{v}}_k &= \underset{\tilde{\mathbf{v}}}{\operatorname{argmin}} \frac{\lambda}{2\beta} \|(\tilde{\mathbf{x}}_k + \tilde{\mathbf{u}}_{k-1}) - \tilde{\mathbf{v}}\|_2^2 + s(\tilde{\mathbf{v}}), \\ \tilde{\mathbf{u}}_k &= \tilde{\mathbf{u}}_{k-1} + (\tilde{\mathbf{x}}_k - \tilde{\mathbf{v}}_k). \end{aligned} \quad (6)$$

Note that the first step in (6) is just solving a least squares (LS) problem and the third step is a simple update. The second step is more interesting. It describes obtaining $\tilde{\mathbf{v}}_k$ using a white Gaussian denoiser with noise variance of $\sigma^2 = \beta/\lambda$, applied on the image $\tilde{\mathbf{x}}_k + \tilde{\mathbf{u}}_{k-1}$. This can be written compactly as $\tilde{\mathbf{v}}_k = \mathcal{D}(\tilde{\mathbf{x}}_k + \tilde{\mathbf{u}}_{k-1}; \sigma)$, where $\mathcal{D}(\cdot; \sigma)$ is a denoising operator. Since general denoising algorithms can be used to implement the operator $\mathcal{D}(\cdot; \sigma)$, the P&P method does not require knowing or explicitly specifying the prior function $s(\mathbf{x})$. Instead, $s(\mathbf{x})$ is implicitly defined through the choice of $\mathcal{D}(\cdot; \sigma)$. The obtained P&P algorithm is presented in Algorithm 1.

From ADMM theory, *global convergence* (i.e. iterations approach feasibility and objective reaches its optimal value) is ensured if $\ell(\mathbf{x})$ and $s(\mathbf{x})$ are convex, closed, proper, and the unaugmented Lagrangian has a saddle point [17]. Global convergence of P&P is proved for a denoiser $\mathcal{D}(\cdot; \sigma)$ that has a symmetric gradient and is non-expansive [10]. However, the latter is difficult to be proved, and well-known denoisers such as BM3D [1], K-SVD [2], and standard NLM [3], lead to good results despite violating these conditions. Another type of convergence is *fixed point*

Algorithm 1: Plug and Play (P&P)

Input: \mathbf{H} , \mathbf{y} , σ_n , denoising operator $\mathcal{D}(\cdot; \sigma)$, stopping criterion. $\mathbf{y} = \mathbf{H}\mathbf{x} + \mathbf{e}$, such that $\mathbf{e} \sim \mathcal{N}(\mathbf{0}, \sigma_n^2 \mathbf{I}_m)$ and \mathbf{x} is an unknown signal whose prior model is specified by $\mathcal{D}(\cdot; \sigma)$.

Output: $\hat{\mathbf{x}}$ an estimate for \mathbf{x} .

Initialize: $\tilde{\mathbf{v}}_0 =$ some initialization, $\tilde{\mathbf{u}}_0 = \mathbf{0}$, $k = 0$, some initialization for β and λ .

while *stopping criterion not met* **do**

$k = k + 1;$

$\tilde{\mathbf{x}}_k = (\mathbf{H}^T \mathbf{H} + \lambda \sigma_n^2 \mathbf{I}_n)^{-1} (\mathbf{H}^T \mathbf{y} + \lambda \sigma_n^2 (\tilde{\mathbf{v}}_{k-1} - \tilde{\mathbf{u}}_{k-1}));$

$\tilde{\mathbf{v}}_k = \mathcal{D}(\tilde{\mathbf{x}}_k + \tilde{\mathbf{u}}_{k-1}; \sqrt{\beta/\lambda});$

$\tilde{\mathbf{u}}_k = \tilde{\mathbf{u}}_{k-1} + (\tilde{\mathbf{x}}_k - \tilde{\mathbf{v}}_k);$

end

$\hat{\mathbf{x}} = \tilde{\mathbf{x}}_k;$

convergence, which guarantees that an iterative algorithm asymptotically enters a steady state. A modified version of P&P, where the ADMM parameter λ increases between iterations, is guaranteed to have such a convergence under some mild conditions on the denoiser [16].

The P&P method is not free of drawbacks. Its main difficulties are the large number of iterations, which is often required by the P&P to converge to a good solution, and the setting of the design parameters β and λ , which is not always clear and strongly affects the performance.

III. THE PROPOSED ALGORITHM

In this work we take another strategy for solving inverse problems using denoising algorithms. We start with formulating the cost function (2) in somewhat strange but equivalent way

$$f(\tilde{\mathbf{x}}) = \frac{1}{2\sigma_n^2} \|\mathbf{H}(\mathbf{H}^\dagger \mathbf{y} - \tilde{\mathbf{x}})\|_2^2 + s(\tilde{\mathbf{x}}) = \frac{1}{2\sigma_n^2} \|\mathbf{H}^\dagger \mathbf{y} - \tilde{\mathbf{x}}\|_{\mathbf{H}^T \mathbf{H}}^2 + s(\tilde{\mathbf{x}}), \quad (7)$$

where

$$\mathbf{H}^\dagger \triangleq \mathbf{H}^T (\mathbf{H} \mathbf{H}^T)^{-1} \quad (8)$$

$$\|\mathbf{u}\|_{\mathbf{H}^T \mathbf{H}}^2 \triangleq \mathbf{u}^T \mathbf{H}^T \mathbf{H} \mathbf{u}. \quad (9)$$

Note that \mathbf{H}^\dagger is the pseudoinverse of the full row rank matrix \mathbf{H} , and $\|\mathbf{u}\|_{\mathbf{H}^T \mathbf{H}}$ is not a real norm, since $\mathbf{H}^T \mathbf{H}$ is not a positive definite matrix in our case. Moreover, as mentioned above, since the null space of $\mathbf{H}^T \mathbf{H}$ is not empty, the prior $s(\tilde{\mathbf{x}})$ is essential in order to obtain a meaningful solution.

The optimization problem $\min_{\tilde{\mathbf{x}}} f(\tilde{\mathbf{x}})$ can be equivalently written as

$$\min_{\tilde{\mathbf{x}}, \tilde{\mathbf{y}}} \frac{1}{2\sigma_n^2} \|\tilde{\mathbf{y}} - \tilde{\mathbf{x}}\|_{\mathbf{H}^T \mathbf{H}}^2 + s(\tilde{\mathbf{x}}) \quad \text{s.t.} \quad \tilde{\mathbf{y}} = \mathbf{H}^\dagger \mathbf{y}. \quad (10)$$

Note that due to the degenerate constraint, the solution for $\tilde{\mathbf{y}}$ is trivial $\tilde{\mathbf{y}} = \mathbf{H}^\dagger \mathbf{y}$.

Now, we make two major modifications to the above optimization problem. The basic idea is to loose the variable $\tilde{\mathbf{y}}$ in a restricted manner, that can facilitate the estimation of $\tilde{\mathbf{x}}$. First, we give some degrees of freedom to $\tilde{\mathbf{y}}$ by using the constraint $\mathbf{H}\tilde{\mathbf{y}} = \mathbf{y}$ instead of $\tilde{\mathbf{y}} = \mathbf{H}^\dagger \mathbf{y}$. Next, we turn to prevent large components of $\tilde{\mathbf{y}}$ in the null space of \mathbf{H} that may strongly disagree with the prior $s(\tilde{\mathbf{x}})$. We do it by replacing the multiplication by $\frac{1}{\sigma_n^2} \mathbf{H}^T \mathbf{H}$ in the fidelity term, which implies projection onto a subspace, with multiplication by $\frac{1}{(\sigma_n + \delta)^2} \mathbf{I}_n$ that implies a full dimensional space, where δ is a design parameter.

This leads to the following optimization problem

$$\min_{\tilde{\mathbf{x}}, \tilde{\mathbf{y}}} \frac{1}{2(\sigma_n + \delta)^2} \|\tilde{\mathbf{y}} - \tilde{\mathbf{x}}\|_2^2 + s(\tilde{\mathbf{x}}) \quad \text{s.t.} \quad \mathbf{H}\tilde{\mathbf{y}} = \mathbf{y}. \quad (11)$$

Note that δ introduces a tradeoff. On the one hand, exaggerated value of δ should be avoided, as it may over-reduce the effect of the fidelity term. On the other hand, too small value of $(\sigma_n + \delta)^2$ may over-penalize $\tilde{\mathbf{x}}$ unless it is very close to the affine subspace $\{\mathbf{H}\mathbb{R}^n = \mathbf{y}\}$. This limits the effective feasible set of $\tilde{\mathbf{x}}$ in problem (11), such that it may not include potential solutions of the original problem (10). Therefore, we suggest setting the value of δ as

$$\begin{aligned} \delta &= \underset{\tilde{\delta}}{\operatorname{argmin}} (\sigma_n + \tilde{\delta})^2 \\ \text{s.t.} \quad &\frac{1}{\sigma_n^2} \|\mathbf{H}^\dagger \mathbf{y} - \tilde{\mathbf{x}}\|_{\mathbf{H}^T \mathbf{H}} \geq \frac{1}{(\sigma_n + \tilde{\delta})^2} \|\tilde{\mathbf{y}} - \tilde{\mathbf{x}}\|_2 \quad \forall \tilde{\mathbf{x}}, \tilde{\mathbf{y}} \in \mathcal{S}_{(11)}, \end{aligned} \quad (12)$$

where $\mathcal{S}_{(11)}$ denotes the feasible set of problem (11). Note that the feasibility of $\tilde{\mathbf{x}}$ is dictated by $s(\tilde{\mathbf{x}})$ and the feasibility of $\tilde{\mathbf{y}}$ is dictated by the constraint in (11). The problem of obtaining such value for δ (or an approximation) is discussed in Section IV-A, where a relaxed version of the condition in (12) is presented.

Assuming that δ solves (12), the property that $\frac{1}{\sigma_n^2} \|\mathbf{H}^\dagger \mathbf{y} - \tilde{\mathbf{x}}\|_{\mathbf{H}^T \mathbf{H}} \approx \frac{1}{(\sigma_n + \delta)^2} \|\tilde{\mathbf{y}} - \tilde{\mathbf{x}}\|_2$ for feasible $\tilde{\mathbf{x}}$ and $\tilde{\mathbf{y}}$, together with the fact that $\tilde{\mathbf{y}} = \mathbf{H}^\dagger \mathbf{y}$ is one of the solutions of the underdetermined system $\mathbf{H}\tilde{\mathbf{y}} = \mathbf{y}$, prevents increasing the penalty on potential solutions of the original optimization problem (10). Therefore, roughly speaking, we do not lose solutions when we solve (11) instead of (10).

We solve (11) using alternating minimization. Iteratively, $\tilde{\mathbf{x}}_k$ is estimated by solving

$$\tilde{\mathbf{x}}_k = \underset{\tilde{\mathbf{x}}}{\operatorname{argmin}} \frac{1}{2(\sigma_n + \delta)^2} \|\tilde{\mathbf{y}}_{k-1} - \tilde{\mathbf{x}}\|_2^2 + s(\tilde{\mathbf{x}}), \quad (13)$$

and $\tilde{\mathbf{y}}_k$ is estimated by solving

$$\tilde{\mathbf{y}}_k = \underset{\tilde{\mathbf{y}}}{\operatorname{argmin}} \|\tilde{\mathbf{y}} - \tilde{\mathbf{x}}_k\|_2^2 \quad \text{s.t.} \quad \mathbf{H}\tilde{\mathbf{y}} = \mathbf{y}, \quad (14)$$

which describes a projection of $\tilde{\mathbf{x}}_k$ onto the affine subspace $\{\mathbf{H}\mathbb{R}^n = \mathbf{y}\}$, and has a closed-form solution

$$\tilde{\mathbf{y}}_k = \mathbf{H}^\dagger \mathbf{y} + (\mathbf{I}_n - \mathbf{H}^\dagger \mathbf{H}) \tilde{\mathbf{x}}_k. \quad (15)$$

Similarly to the P&P technique, (13) describes obtaining $\tilde{\mathbf{x}}_k$ using a white Gaussian denoiser with noise variance of $\sigma^2 = (\sigma_n + \delta)^2$, applied on the image $\tilde{\mathbf{y}}_{k-1}$, and can be written compactly as $\tilde{\mathbf{x}}_k = \mathcal{D}(\tilde{\mathbf{y}}_{k-1}; \sigma)$, where $\mathcal{D}(\cdot; \sigma)$

is a denoising operator. Moreover, as in the case of the P&P, the proposed method does not require knowing or explicitly specifying the prior function $s(\mathbf{x})$. Instead, $s(\mathbf{x})$ is implicitly defined through the choice of $\mathcal{D}(\cdot; \sigma)$.

The variable $\tilde{\mathbf{y}}_k$ is expected to be closer to the true signal \mathbf{x} than the raw observations \mathbf{y} . Thus, our algorithm alternates between estimating the signal and using this estimation in order to obtain improved measurements (that also comply with the original observations \mathbf{y}). The proposed algorithm, which we call Iterative Denoising and Backward Projections (IDBP), is presented in Algorithm 2.

Algorithm 2: Iterative Denoising and Backward Projections (IDBP)

Input: $\mathbf{H}, \mathbf{y}, \sigma_n$, denoising operator $\mathcal{D}(\cdot; \sigma)$, stopping criterion. $\mathbf{y} = \mathbf{H}\mathbf{x} + \mathbf{e}$, such that $\mathbf{e} \sim \mathcal{N}(\mathbf{0}, \sigma_n^2 \mathbf{I}_m)$ and \mathbf{x} is an unknown signal whose prior model is specified by $\mathcal{D}(\cdot; \sigma)$.

Output: $\hat{\mathbf{x}}$ an estimate for \mathbf{x} .

Initialize: $\tilde{\mathbf{y}}_0 =$ some initialization, $k = 0$, δ approx. satisfying (12).

while *stopping criterion not met* **do**

$k = k + 1;$

$\tilde{\mathbf{x}}_k = \mathcal{D}(\tilde{\mathbf{y}}_{k-1}; \sigma_n + \delta);$

$\tilde{\mathbf{y}}_k = \mathbf{H}^\dagger \mathbf{y} + (\mathbf{I}_n - \mathbf{H}^\dagger \mathbf{H}) \tilde{\mathbf{x}}_k;$

end

$\hat{\mathbf{x}} = \tilde{\mathbf{x}}_k;$

IV. MATHEMATICAL ANALYSIS OF THE ALGORITHM

A. Setting the value of the parameter δ

Setting the value of δ that solves (12) is required for simple theoretical justification of our method. However, it is not clear how to obtain such δ in general. Therefore, in order to relax the condition in (12), that should be satisfied by all $\tilde{\mathbf{x}}$ and $\tilde{\mathbf{y}}$ in $\mathcal{S}_{(11)}$, we can focus only on the sequences $\{\tilde{\mathbf{x}}_k\}$ and $\{\tilde{\mathbf{y}}_k\}$ generated by the proposed alternating minimization process. Then, we can use the following proposition.

Proposition 1. *Set $\delta = \tilde{\delta}$. If there exist an iteration k of IDBP that violates the following condition*

$$\frac{1}{\sigma_n^2} \|\mathbf{y} - \mathbf{H}\tilde{\mathbf{x}}_k\|_2 \geq \frac{1}{(\sigma_n + \tilde{\delta})^2} \|\mathbf{H}^\dagger(\mathbf{y} - \mathbf{H}\tilde{\mathbf{x}}_k)\|_2, \quad (16)$$

then $\delta = \tilde{\delta}$ also violates the condition in (12).

Proof. Assume that $\tilde{\mathbf{x}}_k$ and $\tilde{\mathbf{y}}_k$ generated by IDBP at some iteration k violate (16), then they also violate the equivalent condition

$$\frac{1}{\sigma_n^2} \|\mathbf{H}^\dagger \mathbf{y} - \tilde{\mathbf{x}}_k\|_{\mathbf{H}^T \mathbf{H}} \geq \frac{1}{(\sigma_n + \tilde{\delta})^2} \|\mathbf{H}^\dagger \mathbf{y} - \mathbf{H}^\dagger \mathbf{H} \tilde{\mathbf{x}}_k\|_2. \quad (17)$$

Note that (17) is obtained simply by plugging (15) into $\tilde{\mathbf{y}}$ in (12). Therefore, $\tilde{\mathbf{x}}_k$ and $\tilde{\mathbf{y}}_k$ also violate the inequality in (12). Finally, it is easy to see that $\tilde{\mathbf{x}}_k$ and $\tilde{\mathbf{y}}_k$ are feasible points of (11), since $\tilde{\mathbf{x}}_k$ is a feasible point of $s(\tilde{\mathbf{x}})$ and $\tilde{\mathbf{y}}_k$ satisfies $\mathbf{H}\tilde{\mathbf{y}}_k = \mathbf{y}$. Therefore, the condition in (12) does not hold for all feasible $\tilde{\mathbf{x}}$ and $\tilde{\mathbf{y}}$, which means that $\delta = \tilde{\delta}$ violates it. \square

Note that (16) can be easily evaluated for each iteration. Thus, violation of (12) can be spotted (by violation of (16)) and used for stopping the process, increasing δ and running the algorithm again. Of course, the opposite direction does not hold. Even when (16) is satisfied for all iterations, it does not guarantee satisfying (12). However, the relaxed condition (16) provides an easy way to set δ with an approximation to the solution of (12), which gives very good results in our experiments.

In the special case of the inpainting problem, (16) becomes ridiculously simple. Since \mathbf{H} is a selection of m rows of \mathbf{I}_n , it follows that $\mathbf{H}^\dagger = \mathbf{H}^T$, which is an $n \times m$ matrix that merely pads with $n - m$ zeros the vector on which it is applied. Therefore, $\|\mathbf{y} - \mathbf{H}\tilde{\mathbf{x}}_k\|_2 = \|\mathbf{H}^\dagger(\mathbf{y} - \mathbf{H}\tilde{\mathbf{x}}_k)\|_2$, implying that $\delta = 0$ satisfies (16) in this case. Obviously, if $\sigma_n = 0$, a small positive δ is required in order to prevent the algorithm from getting stuck (because in this case $\sigma = \sigma_n + \delta = 0$).

Condition (16) is more complex when considering the deblurring problem. In this case \mathbf{H} is an ill-conditioned matrix. Therefore \mathbf{H}^\dagger must be approximated, either by approximating \mathbf{H} by a full rank $m \times n$ matrix before computing (8), or by regularized inversion techniques for \mathbf{H} , e.g. standard Tikhonov regularization. A research on how to compute δ in this case is ongoing. We empirically observed that using a fixed value for δ (for all noise levels and blur kernels) exhibits good performance. However, we had to add another parameter ϵ that controls the amount of regularization in the approximation of \mathbf{H}^\dagger , that we slightly change between scenarios (i.e. when \mathbf{H} or σ_n change). This issue is discussed in Section V-B. An interesting observation is that the pairs of (δ, ϵ) which give the best results indeed satisfy condition (16). On the other hand, the pairs of (δ, ϵ) that give bad results often violate this condition (recall that the condition should be met during all iterations). An example of this behavior is given in the end of Section V-B.

B. Analysis of the sequence $\{\tilde{\mathbf{y}}_k\}$

The IDBP algorithm creates the sequence $\{\tilde{\mathbf{y}}_k\}$ that can be interpreted as a sequence of updated measurements. It is desired that $\tilde{\mathbf{y}}_k$ is improved with each iteration, i.e. that $\tilde{\mathbf{x}}_{k+1}$, obtained from $\tilde{\mathbf{y}}_k$, estimates \mathbf{x} better than $\tilde{\mathbf{x}}_k$, which is obtained from $\tilde{\mathbf{y}}_{k-1}$.

Assuming that the result of the denoiser, denoted by $\bar{\mathbf{x}}$, is perfect, i.e. $\bar{\mathbf{x}} = \mathbf{x}$, we get from (15)

$$\bar{\mathbf{y}} = \mathbf{H}^\dagger \mathbf{y} + (\mathbf{I}_n - \mathbf{H}^\dagger \mathbf{H}) \bar{\mathbf{x}} = \mathbf{H}^\dagger (\mathbf{H} \mathbf{x} + \mathbf{e}) + (\mathbf{I}_n - \mathbf{H}^\dagger \mathbf{H}) \mathbf{x} = \mathbf{x} + \mathbf{H}^\dagger \mathbf{e}. \quad (18)$$

The last equality describes a model that has only noise (possibly colored), and is much easier to deal with than the original model (1). Therefore, $\bar{\mathbf{y}}$ can be considered as the optimal improved measurements that our algorithm can

achieve. As we wish to make no specific assumptions on the denoising scheme $\tilde{\mathbf{x}}_k = \mathcal{D}(\tilde{\mathbf{y}}_{k-1}; \sigma)$, improvement of $\{\tilde{\mathbf{y}}_k\}$ will be measured by the Euclidean distance to $\bar{\mathbf{y}}$.

Denote by $\mathbf{P}_H \triangleq \mathbf{H}^\dagger \mathbf{H}$ the orthogonal projection onto the row space of \mathbf{H} , and its orthogonal complement by $\mathbf{Q}_H \triangleq \mathbf{I}_n - \mathbf{H}^\dagger \mathbf{H}$. The updated measurements $\tilde{\mathbf{y}}_k$ are always consistent with \mathbf{y} on $\mathbf{P}_H \mathbf{x}$, and do not depend on $\mathbf{P}_H \tilde{\mathbf{x}}_k$, as can be seen from

$$\begin{aligned} \tilde{\mathbf{y}}_k &= \mathbf{H}^\dagger (\mathbf{H} \mathbf{x} + \mathbf{e}) + \mathbf{Q}_H \tilde{\mathbf{x}}_k \\ &= \mathbf{P}_H \mathbf{x} + \mathbf{H}^\dagger \mathbf{e} + \mathbf{Q}_H \tilde{\mathbf{x}}_k. \end{aligned} \quad (19)$$

Thus, the following theorem ensures that iteration k improves the results, provided that $\tilde{\mathbf{x}}_k$ is closer to \mathbf{x} than $\tilde{\mathbf{y}}_{k-1}$ on the null space of \mathbf{H} , i.e.,

$$\|\mathbf{Q}_H(\tilde{\mathbf{x}}_k - \mathbf{x})\|_2 < \|\mathbf{Q}_H(\tilde{\mathbf{y}}_{k-1} - \mathbf{x})\|_2. \quad (20)$$

Theorem 2. *Assuming that (20) holds at the k th iteration of IDBP, then we have*

$$\|\tilde{\mathbf{y}}_k - \bar{\mathbf{y}}\|_2 < \|\tilde{\mathbf{y}}_{k-1} - \bar{\mathbf{y}}\|_2. \quad (21)$$

Proof. Note that

$$\mathbf{Q}_H \tilde{\mathbf{y}}_{k-1} = \mathbf{Q}_H (\mathbf{H}^\dagger \mathbf{y} + \mathbf{Q}_H \tilde{\mathbf{x}}_{k-1}) = \mathbf{Q}_H \tilde{\mathbf{x}}_{k-1}. \quad (22)$$

Equation (21) is obtained by

$$\begin{aligned} \|\tilde{\mathbf{y}}_k - \bar{\mathbf{y}}\|_2 &= \|(\mathbf{P}_H \mathbf{x} + \mathbf{H}^\dagger \mathbf{e} + \mathbf{Q}_H \tilde{\mathbf{x}}_k) - (\mathbf{x} + \mathbf{H}^\dagger \mathbf{e})\|_2 \\ &= \|\mathbf{Q}_H(\tilde{\mathbf{x}}_k - \mathbf{x})\|_2 \\ &< \|\mathbf{Q}_H(\tilde{\mathbf{x}}_{k-1} - \mathbf{x})\|_2 \\ &= \|(\mathbf{P}_H \mathbf{x} + \mathbf{H}^\dagger \mathbf{e} + \mathbf{Q}_H \tilde{\mathbf{x}}_{k-1}) - (\mathbf{x} + \mathbf{H}^\dagger \mathbf{e})\|_2 \\ &= \|\tilde{\mathbf{y}}_{k-1} - \bar{\mathbf{y}}\|_2, \end{aligned} \quad (23)$$

where the inequality follows from (20) and (22). \square

A denoiser that makes use of a good prior (and suitable σ) is expected to satisfy (20), at least in early iterations. For example, in the inpainting problem \mathbf{Q}_H is associated with the missing pixels, and in the deblurring problem \mathbf{Q}_H is associated with the data that suffer the greatest loss by the blur kernel. Therefore, in both cases $\mathbf{Q}_H \tilde{\mathbf{x}}_k$ is expected to be closer to $\mathbf{Q}_H \mathbf{x}$ than $\mathbf{Q}_H \tilde{\mathbf{y}}_{k-1}$. Note that if (20) holds for all iterations, then Theorem 2 ensures monotonic improvement and convergence of $\{\tilde{\mathbf{y}}_k\}$, and thus, a fixed point convergence of IDBP. However, note that it does not guarantee that $\bar{\mathbf{y}}$ is the limit of the sequence $\{\tilde{\mathbf{y}}_k\}$.

C. Recovery guarantees

Similar to P&P, in order to prove more than a fixed point convergence of IDBP, strict assumptions on the denoising scheme are required. For global convergence of P&P, it is enough to assume that the denoiser is non-expansive and has a symmetric gradient [10], which allows using the proximal mapping theorem of Moreau [18]. However, non-expansiveness property of a denoiser is very demanding, as it requires that for a given noise level σ we have

$$\|\mathcal{D}(z_1; \sigma) - \mathcal{D}(z_2; \sigma)\|_2 \leq K_\sigma \|z_1 - z_2\|_2, \quad (24)$$

for any z_1 and z_2 in \mathbb{R}^n , with $K_\sigma \leq 1$.

In this work we take a different route that exploits the structure of the IDBP algorithm, where the denoiser's output is always projected onto the null space of \mathbf{H} . Instead of assuming (20), we use the following assumptions:

Condition 1. *The denoiser is bounded, in the sense of*

$$\|\mathcal{D}(z; \sigma) - z\|_2 \leq \sigma B, \quad (25)$$

for any $z \in \mathbb{R}^n$, where B is a universal constant independent of σ .

Condition 2. *For a given noise level σ , the projection of the denoiser onto the null space of \mathbf{H} is a contraction, i.e., it satisfies*

$$\|\mathbf{Q}_H \mathcal{D}(z_1; \sigma) - \mathbf{Q}_H \mathcal{D}(z_2; \sigma)\|_2 \leq K_\sigma \|z_1 - z_2\|_2, \quad (26)$$

for any $z_1 \neq z_2$ in \mathbb{R}^n , where $K_\sigma < 1$, and $\mathbf{Q}_H \triangleq \mathbf{I}_n - \mathbf{H}^\dagger \mathbf{H}$.

Condition 1 implies that $\mathcal{D}(z; 0) = z$, as can be expected from a denoiser. Thus, it prevents considering a trivial mapping, e.g. $\mathcal{D}(z; \sigma) = \mathbf{0}$ for all z , which trivially satisfies Condition 2. Regarding the second condition, even though it describes a contraction, it considers the operator $\mathbf{Q}_H \mathcal{D}(\cdot; \sigma)$. Therefore, for some cases of \mathbf{H} , it might be weaker than non-expansiveness of $\mathcal{D}(\cdot; \sigma)$. Our main recovery guarantee is given in the following theorem.

Theorem 3. *Let $\mathbf{y} = \mathbf{H}\mathbf{x} + \mathbf{e}$, apply IDBP with some σ for the denoising operation, and assume that Condition 1 holds. Assume also that Condition 2 holds for this choice of σ . Then, with the notation of IDBP we have*

$$\|\tilde{\mathbf{x}}_{k+1} - \mathbf{x}\|_2 \leq K_\sigma^k \|\tilde{\mathbf{y}}_0 - \bar{\mathbf{y}}\|_2 + \frac{1}{1 - K_\sigma} \|\mathbf{H}^\dagger \mathbf{e}\|_2 + C_\sigma, \quad (27)$$

where $\bar{\mathbf{y}} = \mathbf{x} + \mathbf{H}^\dagger \mathbf{e}$ and $C_\sigma \triangleq (\frac{1}{1 - K_\sigma} + 5)\sigma B$.

The proof of Theorem 3 appears in the appendix.

Theorem 3 provides an upper bound on the error of IDBP w.r.t. the true signal \mathbf{x} . It can be seen that for a fixed number of iterations, a bounded denoiser with a smaller K_σ is expected to perform better. If K_σ is close to 1, more iterations will reduce the first term in the bound, but not the second term, which may be an artifact of our proof. The third term C_σ may suggest using IDBP with the smallest possible σ . However, Condition 2 implies that smaller σ yields larger K_σ , since the denoiser has a smaller effect on its input, and (26) needs to be satisfied for

any two signals z_1 and z_2 . Still, assuming that the effect on K_σ is small and can be compensated by using more iterations, smaller σ is beneficial. The last observation on C_σ agrees with our suggestion to choose δ according to (12), where $\sigma = \sigma_n + \delta$ is minimized under a constraint that aims to prevent losing solutions when (11) is being solved instead of (10).

To the best of our knowledge, there is no equivalent result like Theorem 3 for P&P, as its existing convergence guarantees refer to approaching a minimizer of the original cost function (2), which is not necessarily identical to \mathbf{x} . Therefore, even though we propose an alternative method to minimize (2), we choose to consider IDBP error w.r.t. the true \mathbf{x} . Note though that the proof technique we show here can be also used to bound the Euclidean distance between the IDBP estimation and a (pre-computed) solution of (2) with only minor technical changes.

V. EXPERIMENTS

We demonstrate the usage of IDBP for two test scenarios: the inpainting and the deblurring problems. We compare the IDBP performance to P&P and another algorithm that has been specially tailored for each problem [6], [19]. In all experiments we use BM3D [1] as the denoising algorithm for IDBP and P&P. We use the following eight test images in all experiments: *cameraman*, *house*, *peppers*, *Lena*, *Barbara*, *boat*, *hill* and *couple*. Their intensity range is 0-255.

A. Image inpainting

In the image inpainting problem, \mathbf{H} is a selection of m rows of \mathbf{I}_n and $\mathbf{H}^\dagger = \mathbf{H}^T$, which simplifies both P&P and IDBP. In P&P, the first step can be solved for each pixel individually. In IDBP, $\tilde{\mathbf{y}}_k$ is obtained merely by taking the observed pixels from \mathbf{y} and the missing pixels from $\tilde{\mathbf{x}}_k$. For both methods we use the result of a simple median scheme as their initialization (for $\tilde{\mathbf{v}}_0$ in P&P and for $\tilde{\mathbf{y}}_0$ in IDBP). It is also possible to alternatively use $\mathbf{H}^T \mathbf{y}$ for initialization, but then many more iterations are required. Note that the computational cost of each iteration of P&P and IDBP is of the same scale, dominated by the complexity of the denoising operation.

The first experiment demonstrates the performance of IDBP, P&P and inpainting based on Image Processing using Patch Ordering (IPPO) approach [19], for the noiseless case ($\sigma_n = 0$) with 80% missing pixels, selected at random. The parameters of IPPO are set exactly as in [19], where the same scenario is examined. The parameters of P&P are optimized for best reconstruction quality. We use $\beta = 1$, $\lambda = 10/255$ and 150 iterations. Also, for P&P we assume that the noise standard deviation is 0.001, i.e. nonzero, in order to compute $\tilde{\mathbf{x}}_k$.

Considering IDBP, in Section IV-A, it is suggested that $\delta = 0$. However, since in this case $\sigma_n + \delta = 0$, a small positive δ , e.g. $\delta = 1$, is required. Indeed, this setting gives good performance, but also requires ten times more iterations than P&P. Therefore, we use an alternative approach. We set $\delta = 5$, which allows us to use only 150 iterations (same as P&P), but take the last $\tilde{\mathbf{y}}_k$ as the final estimate, which is equivalent to performing the last denoising with the recommended $\delta = 0$. Figure 1 shows the results of both IDBP implementations for the *house* image. It approves that the alternative implementation performs well and requires significantly less iterations (note

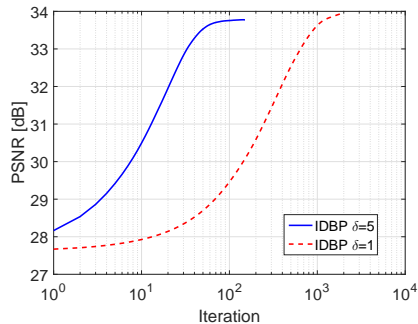


Fig. 1: IDBP recovery (PSNR vs. iteration) of *house* test image with 80% missing pixels and no noise.

TABLE I: Inpainting results (PSNR in dB) for 80% missing pixels and $\sigma_n = 0$.

	<i>camera.</i>	<i>house</i>	<i>peppers</i>	<i>Lena</i>	<i>Barbara</i>	<i>boat</i>	<i>hill</i>	<i>couple</i>
IPPO	24.78	32.64	27.98	31.84	29.89	28.17	29.47	28.22
P&P	24.83	34.72	26.88	32.41	25.68	28.83	29.95	29.01
IDBP	24.86	33.78	26.86	32.13	25.55	28.51	29.74	28.80

that the x-axis has a logarithmic scale). Therefore, for the comparison of the different inpainting methods in this experiment, we use the alternative implementation of IDBP with $\delta = 5$. The empirical behavior observed here, agrees with the theoretical observation at the end of Section IV-C: larger $\sigma = \sigma_n + \delta$ requires less iterations (due to smaller K_σ) but results in higher error. Note also that it is possible to decrease δ as the iterations increase. However, in this work we aim at demonstrating IDBP performance with minimal parameter tuning as possible.

The results of the three algorithms are given in Table I. IDBP is usually better than IPPO, but slightly inferior to P&P. This is the cost of enhancing IDBP by setting δ to a value which is significantly larger than zero. However, this observation also hints that IDBP may shine for noisy measurements, where $\delta = 0$ can be used without increasing the number of iterations. We also remark that IPPO gives the best results for *peppers* and *Barbara* because in these images P&P and IDBP require more than the fixed 150 iterations.

The second experiment demonstrates the performance of IDBP and P&P with 80% missing pixels, as before, but this time $\sigma_n = 10$. Noisy inpainting has not been implemented yet by IPPO [19]. The parameters of P&P that give us the best results are $\beta = 0.8$, $\lambda = 5/255$ and 150 iterations. Using the same parameter values as before deteriorates the performance significantly. Contrary to P&P, in this experiment tuning the parameters of IDBP can be avoided. We follow Section IV-A and set $\delta = 0$. Moreover, IDBP now requires only 75 iterations, half the number of P&P. The results are given in Table II. P&P is slightly inferior to IDBP, despite having twice the number of iterations and a burdensome parameter tuning. The results for *house* are also presented in Figure 2, where it can be seen that P&P reconstruction suffers from more artifacts (e.g. ringing artifacts near the right window).

We repeat the last experiment with slightly increased noise level of $\sigma_n = 12$, but still use the same parameter tuning for P&P, which is optimized for $\sigma_n = 10$ (i.e. $\beta = 0.8$, $\lambda = 5/255$ and the fixed $\delta = 0$). This situation

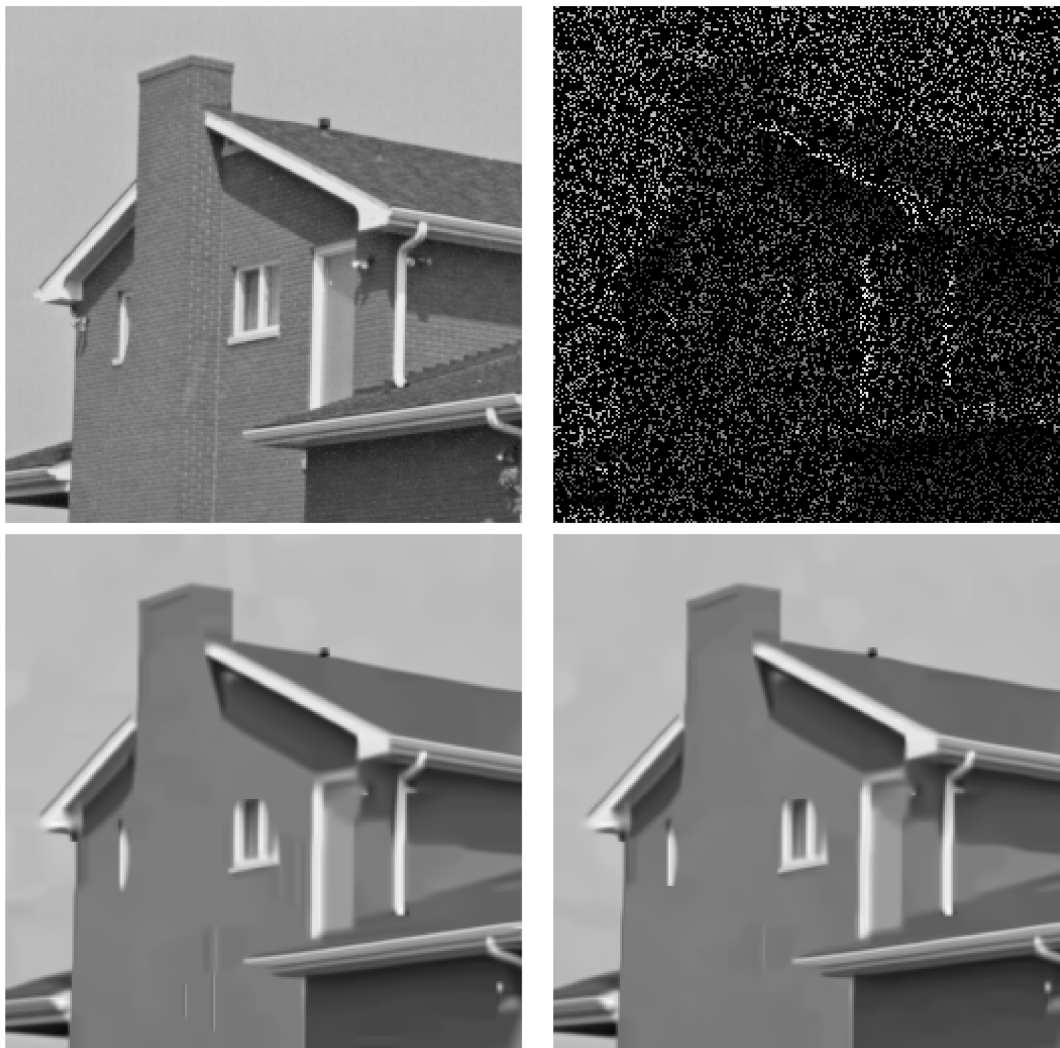


Fig. 2: Recovery of *house* image with 80% missing pixels and $\sigma_n = 10$. From left to right and from top to bottom: original image, subsampled and noisy image, reconstruction of P&P, and reconstruction of the proposed IDBP.

TABLE II: Inpainting results (PSNR in dB) for 80% missing pixels and $\sigma_n = 10$.

	<i>camera.</i>	<i>house</i>	<i>peppers</i>	<i>Lena</i>	<i>Barbara</i>	<i>boat</i>	<i>hill</i>	<i>couple</i>
P&P	24.55	31.53	26.16	30.10	24.45	27.01	27.94	27.23
IDBP	24.68	31.62	26.13	30.14	25.03	27.02	28.00	27.22

is often encountered in practice, when calibrating a system for all possible scenarios is impossible. The results are given in Table III. The IDBP clearly outperforms P&P in this case. This experiment clearly shows the main advantage of our algorithm over P&P as it is less sensitive to parameter tuning.

TABLE III: Inpainting results (PSNR in dB) for 80% missing pixels and $\sigma_n = 12$, with the same parameters as in Table II (tuned for $\sigma_n = 10$).

	<i>camera.</i>	<i>house</i>	<i>peppers</i>	<i>Lena</i>	<i>Barbara</i>	<i>boat</i>	<i>hill</i>	<i>couple</i>
P&P	24.43	30.78	25.80	29.47	24.12	26.53	27.44	26.71
IDBP	24.51	31.14	25.92	29.69	25.06	26.64	27.61	26.77

B. Image deblurring

In the image deblurring problem, for a circular shift-invariant blur operator whose kernel is \mathbf{h} , both P&P and IDBP can be efficiently implemented using Fast Fourier Transform (FFT). In P&P, $\tilde{\mathbf{x}}_k$ can be computed by

$$\tilde{\mathbf{x}}_k = \mathcal{F}^{-1} \left\{ \frac{\mathcal{F}^*\{\mathbf{h}\}\mathcal{F}\{\mathbf{y}\} + \lambda\sigma_n^2\mathcal{F}\{\tilde{\mathbf{v}}_{k-1} - \tilde{\mathbf{u}}_{k-1}\}}{|\mathcal{F}\{\mathbf{h}\}|^2 + \lambda\sigma_n^2} \right\}. \quad (28)$$

where $\mathcal{F}\{\cdot\}$ denotes the FFT operator, $\mathcal{F}^{-1}\{\cdot\}$ denotes the inverse FFT operator.

Recall that \mathbf{H} is an ill-conditioned $n \times n$ matrix. Therefore, In IDBP we replace \mathbf{H}^\dagger with a regularized inversion of \mathbf{H} , using standard Tikhonov regularization, which is given in the Fourier domain by

$$\tilde{\mathbf{g}} \triangleq \frac{\mathcal{F}^*\{\mathbf{h}\}}{|\mathcal{F}\{\mathbf{h}\}|^2 + \epsilon \cdot \sigma_n^2}, \quad (29)$$

where ϵ is a parameter that controls the amount of regularization in the approximation of \mathbf{H}^\dagger . Then, $\tilde{\mathbf{y}}_k$ in IDBP can be computed by

$$\tilde{\mathbf{y}}_k = \mathcal{F}^{-1}\{\tilde{\mathbf{g}}\mathcal{F}\{\mathbf{y}\}\} + \tilde{\mathbf{x}}_k - \mathcal{F}^{-1}\{\tilde{\mathbf{g}}\mathcal{F}\{\mathbf{h}\}\mathcal{F}\{\tilde{\mathbf{x}}_k\}\}. \quad (30)$$

While a research on how to compute δ in this case is ongoing, we empirically observed that using a fixed value $\delta = 5$ exhibits good performance with only slightly changing ϵ between the examined scenarios (i.e. different configurations of \mathbf{H} and σ_n). Lastly, we remark that we use trivial initialization in both methods, i.e. $\tilde{\mathbf{v}}_0 = \mathbf{y}$ in P&P and $\tilde{\mathbf{y}}_0 = \mathbf{y}$ in IDBP. Similarly to inpainting, the computational cost of each iteration of P&P and IDBP is on the same scale, dominated by the complexity of the denoising operation.

We consider four deblurring scenarios used as benchmarks in many publications (e.g. [5], [6]). The blur kernel $h(x_1, x_2)$ and noise level of each scenario are summarized in Table IV. The kernels are normalized such that $\sum_{x_1, x_2} h(x_1, x_2) = 1$. Table V shows the results of IDBP, P&P and the dedicated algorithm BM3D-DEB [6]. For each scenario it shows the input PSNR (i.e. PSNR of \mathbf{y}) and the BSNR (blurred signal-to-noise-ratio, defined as $\text{var}(\mathbf{H}\mathbf{x})/m\sigma_n^2$) for each image, as well as the ISNR (improvement signal-to-noise-ratio) for each method and image, which is the difference between the PSNR of the reconstruction and the input PSNR. Note that in Scenario 3, σ_n^2 is set slightly different for each image, ensuring that the BSNR is 40 dB.

The parameters of BM3D-DEB are set exactly as in [6], where the same scenarios are examined. The parameters of P&P are optimized for each scenario. We have $\beta = \{0.85, 0.85, 0.9, 0.8\}$ and $\lambda = \{2, 1, 3, 1\}/255$, for scenarios 1-4, respectively, and use 50 iterations. IDBP is easier to tune, as we set $\epsilon = \{7\text{e-}3, 4\text{e-}3, 8\text{e-}3, 2\text{e-}3\}$ for scenarios

TABLE IV: Blur kernel and noise variance of different scenarios.

Scenario	$h(x_1, x_2)$	σ_n^2
1	$1/(x_1^2 + x_2^2), x_1, x_2 = -7, \dots, 7$	2
2	$1/(x_1^2 + x_2^2), x_1, x_2 = -7, \dots, 7$	8
3	9×9 uniform	≈ 0.3
4	$[1, 4, 6, 4, 1]^T [1, 4, 6, 4, 1]/256$	49

1-4, respectively, and fixed $\delta = 5$. Also, we use only 20 iterations for IDBP. From Table V, it is clear that IDBP and P&P are highly competitive (arguably, IDBP performs better), and both are much better than BM3D-DEB, which is tailored for the deblurring problem. Figure 3 displays the results for *Lena* in Scenario 2. It can be seen that IDBP reconstruction is the sharpest (e.g. notice the lightning in the right eye).

As mentioned in Section IV-A, we observed that the pairs of (δ, ϵ) which give the best results indeed satisfy condition (16), while the pairs of (δ, ϵ) that give bad results often violate this condition. This behavior is demonstrated for *house* image in Scenario 1. Figure 4a shows the PSNR vs. iteration for several pairs of (δ, ϵ) . The left-hand side of (16) divided by the right-hand side is presented in Figure 4b. If this division is less than 1, even for a single iteration, it means that the original condition in (12) is violated by the associated (δ, ϵ) . Recall that even when the division is higher than 1 for all iterations, it does not guarantee satisfying (12). Therefore, a small margin should be kept, as observed for $(\delta=5, \epsilon=7e-3)$. When the margin further increases, graceful degradation is expected, as observed for $(\delta=7, \epsilon=7e-3)$ and $(\delta=5, \epsilon=10e-3)$.

VI. CONCLUSION

We presented the Iterative Denoising and Backward Projections (IDBP) method for solving linear inverse problems using denoising algorithms. This method, in its general form, has only a single parameter that should be set according to a given condition. We presented mathematical analysis of this strategy and provided a practical way to tune its parameter. Therefore, it can be argued that our method has less parameters that require tuning than the P&P method, especially for the noisy inpainting problem, where the single parameter of the IDBP can be just set to zero. Experiments demonstrated that IDBP is competitive with task-specific algorithms and with the P&P approach for inpainting and deblurring problems.

APPENDIX A

PROOF OF THEOREM 3

We start with proving an auxiliary lemma.

Lemma 4. *Assuming that Condition 1 holds, i.e. $\|\mathcal{D}(z; \sigma) - z\|_2 \leq \sigma B$ for any z , we have*

$$\|\mathcal{D}(z_1; \sigma) - \mathcal{D}(z_2; \sigma)\|_2 \leq \|z_1 - z_2\|_2 + 2\sigma B \quad (31)$$

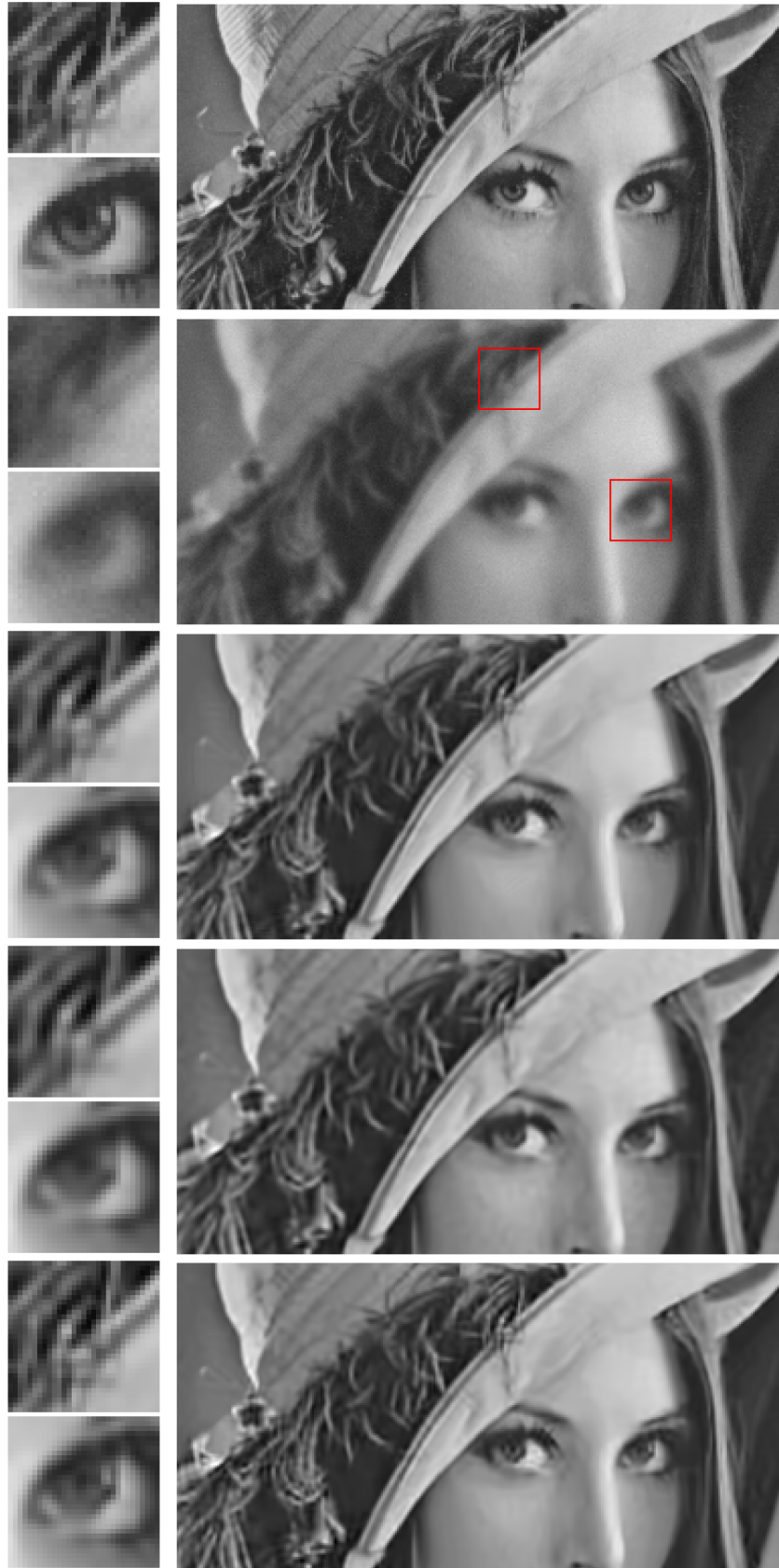


Fig. 3: Deblurring of *Lena* image, Scenario 2. From top to bottom, fragments of: original image, blurred and noisy image, reconstruction of BM3D-DEB, reconstruction of P&P, and reconstruction of the proposed IDBP.

TABLE V: Deblurring inputs (BSNR and input PSNR in dB) and reconstruction results (Improvement SNR in dB for each method) for scenarios 1-4.

Scenario 1	<i>camera.</i>	<i>house</i>	<i>peppers</i>	<i>Lena</i>	<i>Barbara</i>	<i>boat</i>	<i>hill</i>	<i>couple</i>
BSNR	31.87	29.16	29.99	29.89	30.81	29.37	30.19	28.81
input PSNR	22.23	25.61	22.60	27.25	23.34	25.00	26.51	24.87
BM3D-DEB	8.20	9.34	9.58	7.96	7.88	7.35	5.77	7.34
P&P	8.03	9.74	10.02	8.02	6.84	7.48	5.78	7.34
IDBP	8.48	9.82	9.86	8.01	7.65	7.59	5.93	7.46
Scenario 2	<i>camera.</i>	<i>house</i>	<i>peppers</i>	<i>Lena</i>	<i>Barbara</i>	<i>boat</i>	<i>hill</i>	<i>couple</i>
BSNR	25.85	23.14	23.97	23.87	24.79	23.35	24.17	22.79
input PSNR	22.16	25.46	22.53	27.04	23.25	24.88	26.33	24.75
BM3D-DEB	6.46	8.22	7.88	6.55	4.13	5.61	4.46	5.60
P&P	6.06	8.20	8.15	6.49	2.72	5.65	4.46	5.56
IDBP	6.53	8.19	7.67	6.64	3.64	5.91	4.62	5.80
Scenario 3	<i>camera.</i>	<i>house</i>	<i>peppers</i>	<i>Lena</i>	<i>Barbara</i>	<i>boat</i>	<i>hill</i>	<i>couple</i>
BSNR	40.00	40.00	40.00	40.00	40.00	40.00	40.00	40.00
input PSNR	20.77	24.11	21.33	25.84	22.49	23.36	25.04	23.24
BM3D-DEB	8.37	10.94	10.05	7.99	5.91	8.48	6.97	8.79
P&P	9.49	13.17	11.70	9.04	5.36	9.71	7.63	9.98
IDBP	9.55	12.90	11.88	9.00	5.98	9.65	7.66	9.89
Scenario 4	<i>camera.</i>	<i>house</i>	<i>peppers</i>	<i>Lena</i>	<i>Barbara</i>	<i>boat</i>	<i>hill</i>	<i>couple</i>
BSNR	18.53	15.99	17.01	16.47	17.35	16.06	16.68	15.55
input PSNR	24.63	28.06	24.77	28.81	24.22	27.10	27.74	26.94
BM3D-DEB	3.35	5.20	3.31	4.80	2.05	3.35	2.94	3.36
P&P	3.31	5.43	4.95	4.84	1.50	3.42	3.13	3.39
IDBP	3.59	5.66	4.12	5.05	1.95	3.54	3.08	3.52

for any \mathbf{z}_1 and \mathbf{z}_2 in \mathbb{R}^n .

Proof. Using the triangle inequality followed by Condition 1, we get the desired result

$$\begin{aligned}
\|\mathcal{D}(\mathbf{z}_1; \sigma) - \mathcal{D}(\mathbf{z}_2; \sigma)\|_2 &\leq \|\mathcal{D}(\mathbf{z}_1; \sigma) - \mathbf{z}_1\|_2 + \|\mathcal{D}(\mathbf{z}_2; \sigma) - \mathbf{z}_2\|_2 + \|\mathbf{z}_1 - \mathbf{z}_2\|_2 \\
&\leq \|\mathbf{z}_1 - \mathbf{z}_2\|_2 + 2\sigma B.
\end{aligned} \tag{32}$$

□

We now turn to the proof of the theorem.

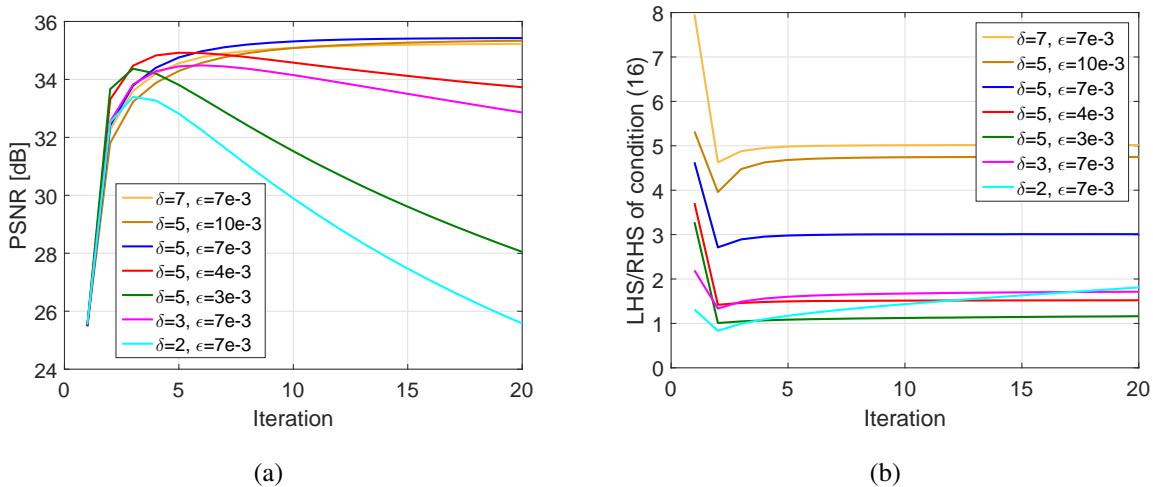


Fig. 4: (a) IDBP deblurring results (PSNR vs. iteration) for *house* in Scenario 1 for several pairs of (δ, ϵ) ; (b) shows the left-hand side of (16) divided by the right-hand side. If any iteration's value is less than 1, it means that the condition in (12) is violated. Since the opposite direction does not hold, it is preferable to keep a margin above 1.

Proof. By $\tilde{\mathbf{x}}_{k+1} = \mathcal{D}(\tilde{\mathbf{y}}_k; \sigma)$, and using the triangle inequality, we have

$$\begin{aligned}
\|\tilde{\mathbf{x}}_{k+1} - \mathbf{x}\|_2 &= \|\mathcal{D}(\tilde{\mathbf{y}}_k; \sigma) - \mathbf{x}\|_2 \\
&\leq \|\mathcal{D}(\tilde{\mathbf{y}}_k; \sigma) - \mathcal{D}(\bar{\mathbf{y}}; \sigma)\|_2 + \|\mathcal{D}(\bar{\mathbf{y}}; \sigma) - \mathcal{D}(\mathbf{x}; \sigma)\|_2 + \|\mathcal{D}(\mathbf{x}; \sigma) - \mathbf{x}\|_2 \\
&\leq \|\tilde{\mathbf{y}}_k - \bar{\mathbf{y}}\|_2 + \|\bar{\mathbf{y}} - \mathbf{x}\|_2 + 5\sigma B \\
&= \|\tilde{\mathbf{y}}_k - \bar{\mathbf{y}}\|_2 + \|\mathbf{H}^\dagger \mathbf{e}\|_2 + 5\sigma B,
\end{aligned} \tag{33}$$

where the second inequality uses Lemma 4 twice, and Condition 1 for the last term, and the last equality follows from the fact that $\bar{\mathbf{y}} = \mathbf{x} + \mathbf{H}^\dagger \mathbf{e}$. We turn to bound the first term in the right-hand side of (33). Because $\tilde{\mathbf{y}}_k = \mathbf{H}^\dagger \mathbf{y} + \mathbf{Q}_H \tilde{\mathbf{x}}_k$ and $\mathbf{y} = \mathbf{H}\mathbf{x} + \mathbf{e}$, we have

$$\begin{aligned}
\|\tilde{\mathbf{y}}_k - \bar{\mathbf{y}}\|_2 &= \|(\mathbf{H}^\dagger \mathbf{H}\mathbf{x} + \mathbf{H}^\dagger \mathbf{e} + \mathbf{Q}_H \tilde{\mathbf{x}}_k) - (\mathbf{x} + \mathbf{H}^\dagger \mathbf{e})\|_2 \\
&= \|\mathbf{Q}_H(\tilde{\mathbf{x}}_k - \mathbf{x})\|_2 \\
&= \|\mathbf{Q}_H(\mathcal{D}(\tilde{\mathbf{y}}_{k-1}; \sigma) - \mathbf{x})\|_2 \\
&\leq \|\mathbf{Q}_H(\mathcal{D}(\tilde{\mathbf{y}}_{k-1}; \sigma) - \mathcal{D}(\bar{\mathbf{y}}; \sigma))\|_2 + \|\mathbf{Q}_H(\mathcal{D}(\bar{\mathbf{y}}; \sigma) - \mathcal{D}(\mathbf{x}; \sigma))\|_2 + \|\mathbf{Q}_H(\mathcal{D}(\mathbf{x}; \sigma) - \mathbf{x})\|_2 \\
&\leq K_\sigma \|\tilde{\mathbf{y}}_{k-1} - \bar{\mathbf{y}}\|_2 + K_\sigma \|\bar{\mathbf{y}} - \mathbf{x}\|_2 + \|\mathcal{D}(\mathbf{x}; \sigma) - \mathbf{x}\|_2 \\
&\leq K_\sigma \|\tilde{\mathbf{y}}_{k-1} - \bar{\mathbf{y}}\|_2 + K_\sigma \|\mathbf{H}^\dagger \mathbf{e}\|_2 + \sigma B,
\end{aligned} \tag{34}$$

where the first inequality follows from the triangle inequality; the second inequality uses Condition 2, i.e. $\mathbf{Q}_H \mathcal{D}(\cdot; \sigma)$ is a contraction, for the first two terms and $\|\mathbf{Q}_H \mathbf{z}\|_2 \leq \|\mathbf{z}\|_2$ for the last term; and the last inequality uses $\bar{\mathbf{y}} = \mathbf{x} + \mathbf{H}^\dagger \mathbf{e}$ and Condition 1. Using recursion (recall that $K_\sigma < 1$) we have

$$\|\tilde{\mathbf{y}}_k - \bar{\mathbf{y}}\|_2 \leq K_\sigma^k \|\tilde{\mathbf{y}}_0 - \bar{\mathbf{y}}\|_2 + \frac{1}{1 - K_\sigma} (K_\sigma \|\mathbf{H}^\dagger \mathbf{e}\|_2 + \sigma B). \tag{35}$$

Finally, substituting (35) in (33) leads to (27). □

REFERENCES

- [1] K. Dabov, A. Foi, V. Katkovnik, and K. Egiazarian, “Image denoising by sparse 3-D transform-domain collaborative filtering,” *IEEE Transactions on image processing*, vol. 16, no. 8, pp. 2080–2095, 2007.
- [2] M. Elad and M. Aharon, “Image denoising via sparse and redundant representations over learned dictionaries,” *IEEE Transactions on Image processing*, vol. 15, no. 12, pp. 3736–3745, 2006.
- [3] A. Buades, B. Coll, and J.-M. Morel, “A review of image denoising algorithms, with a new one,” *Multiscale Modeling & Simulation*, vol. 4, no. 2, pp. 490–530, 2005.
- [4] M. Delbracio and G. Sapiro, “Burst deblurring: Removing camera shake through fourier burst accumulation,” in *Proceedings of the IEEE Conference on Computer Vision and Pattern Recognition*, pp. 2385–2393, 2015.
- [5] J. A. Guerrero-Colón, L. Mancera, and J. Portilla, “Image restoration using space-variant Gaussian scale mixtures in overcomplete pyramids,” *IEEE Transactions on Image Processing*, vol. 17, no. 1, pp. 27–41, 2008.
- [6] K. Dabov, A. Foi, V. Katkovnik, and K. O. Egiazarian, “Image restoration by sparse 3D transform-domain collaborative filtering,” in *SPIE Electronic Imaging '08*, vol. 6812, (San Jose, California, USA), Jan. 2008.
- [7] M. Bertalmio, G. Sapiro, V. Caselles, and C. Ballester, “Image inpainting,” in *Proceedings of the 27th annual conference on Computer graphics and interactive techniques*, pp. 417–424, ACM Press/Addison-Wesley Publishing Co., 2000.
- [8] A. Criminisi, P. Pérez, and K. Toyama, “Region filling and object removal by exemplar-based image inpainting,” *IEEE Transactions on image processing*, vol. 13, no. 9, pp. 1200–1212, 2004.
- [9] S. V. Venkatakrishnan, C. A. Bouman, and B. Wohlberg, “Plug-and-play priors for model based reconstruction,” in *Global Conference on Signal and Information Processing (GlobalSIP), 2013 IEEE*, pp. 945–948, IEEE, 2013.
- [10] S. Sreehari, S. V. Venkatakrishnan, B. Wohlberg, G. T. Buzzard, L. F. Drummy, J. P. Simmons, and C. A. Bouman, “Plug-and-play priors for bright field electron tomography and sparse interpolation,” *IEEE Transactions on Computational Imaging*, vol. 2, no. 4, pp. 408–423, 2016.
- [11] A. Rond, R. Giryes, and M. Elad, “Poisson inverse problems by the plug-and-play scheme,” *Journal of Visual Communication and Image Representation*, vol. 41, pp. 96–108, 2016.
- [12] Y. Dar, A. M. Bruckstein, M. Elad, and R. Giryes, “Postprocessing of compressed images via sequential denoising,” *IEEE Transactions on Image Processing*, vol. 25, no. 7, pp. 3044–3058, 2016.
- [13] T. Meinhardt, M. Möller, C. Hazirbas, and D. Cremers, “Learning proximal operators: Using denoising networks for regularizing inverse imaging problems,” *ICCV*, 2017.
- [14] Y. Romano, M. Elad, and P. Milanfar, “The little engine that could: Regularization by denoising (red),” *arXiv preprint arXiv:1611.02862*, 2016.
- [15] A. M. Teodoro, J. M. Bioucas-Dias, and M. A. Figueiredo, “Image restoration and reconstruction using variable splitting and class-adapted image priors,” in *Image Processing (ICIP), 2016 IEEE International Conference on*, pp. 3518–3522, IEEE, 2016.
- [16] S. H. Chan, X. Wang, and O. A. Elgendy, “Plug-and-play ADMM for image restoration: Fixed-point convergence and applications,” *IEEE Transactions on Computational Imaging*, vol. 3, no. 1, pp. 84–98, 2017.
- [17] S. Boyd, N. Parikh, E. Chu, B. Peleato, and J. Eckstein, “Distributed optimization and statistical learning via the alternating direction method of multipliers,” *Foundations and Trends® in Machine Learning*, vol. 3, no. 1, pp. 1–122, 2011.
- [18] J.-J. Moreau, “Proximité et dualité dans un espace hilbertien,” *Bull. Soc. Math. France*, vol. 93, no. 2, pp. 273–299, 1965.
- [19] I. Ram, M. Elad, and I. Cohen, “Image processing using smooth ordering of its patches,” *IEEE transactions on image processing*, vol. 22, no. 7, pp. 2764–2774, 2013.